

Design optimization of stiffening system for ocean thermal energy conversion (OTEC) cold water pipe (CWP)

Rasgianti^a, Ristiyanto Adiputra^{b,*}, Ariyana Dwiputra Nugraha^a, Nurman Firdaus^b, Ruly Bayu Sitanggang^a, Navik Puryantini^b, Takeshi Yasunaga^c

^a Power Generation System Research Department, PT PLN (Persero) Research Institute, Jakarta Selatan, 12760, Indonesia

^b Research Center for Hydrodynamics Technology, National Research and Innovation Agency (BRIN), Surabaya, 60112, Indonesia

^c Department of Mechanical Engineering, Faculty of Engineering, Osaka Electro-Communication University (OECU), Osaka, 572-8530, Japan

ARTICLE INFO

Keywords:

Ocean thermal energy conversion (OTEC)
Cold water pipe (CWP)
Ring-stiffened pipe
Finite element method
Bending capacity

ABSTRACT

Ocean thermal energy conversion (OTEC) uses heat from seawater to generate electrical energy by utilizing the temperature difference between the surface and deep ocean layer. Cold water pipe (CWP) attached to transport cold seawater over distances of up to 600 m to the plant is susceptible to failures caused by environmental loads. At this point, the CWP should be strengthened to prevent structural failure by inducing ring stiffeners along the pipe. To ensure its structural integrity, this study conducts a design optimization by investigating how the variation of ring stiffening system parameters such as height, thickness, distance between stiffeners, and shape of stiffeners influence the load-carrying capacity of the pipe using a Finite Element Analysis. Initially, the benchmarking procedure is done to ensure the reliability of the FEM modeling. After being verified, the modeling procedure is used for parametric study analyses. Results state that the higher and thicker stiffener ring increases the structural strength. In the case of the ring stiffener distance, as predicted, reducing the spacing between reinforcements is preferable to increasing the bending strength of CWP OTEC. Analyzing the variation of reinforcement height, thickness, and spacing, it was found that thickness had the most significant influence, followed by reinforcement height, and reinforcement spacing had the least. Additionally, changes in the shape of the reinforcement have minimal impact on the flexural strength of the structure when regions of identical moments of inertia exist.

1. Introduction

New renewable energy sources are crucial for addressing environmental issues like pollution, energy shortages, and global warming [1]. These sources are diverse, from solar energy to seawater energy. The potential of seawater energy includes the use of wave kinetic energy, wave kinetic energy of ocean currents and ocean thermal energy [2]. The thermal energy of seawater has the advantage of stable electricity production [3], especially for tropical countries [4]. The increase in Earth's surface temperature due to global warming is increasing the surface temperature of ocean water, which can be harnessed through ocean thermal energy conversion (OTEC) technology [5].

OTEC is a thermal energy conversion technology that exploits the difference between surface and deep sea water temperatures [6]. This temperature gradient is used to evaporate and cool down the working fluid in the Rankine cycle used in OTEC systems, see Fig. 1. For optimal

use of ocean thermal energy, the OTEC device must float at a certain depth in the middle of the ocean, ensuring the necessary temperature difference between the surface and the depth [7].

The OTEC structure consists of several main components, shown in Fig. 2, including the pump system, heat exchanger, cold seawater tank, warm seawater tank, hot water pipe (HWP) and Cold Water Pipe (CWP) [8]. In a 2020 study by Ristiyanto Adiputra et al., an OTEC design with a capacity of 100 MW was proposed [9]. A study found that the OTEC potential in Indonesia's oceans reaches 45 GW, so the implementation of the latter design will require approximately 450 OTEC tankers to fully utilize the thermal energy potential of the Indonesian oceans [4]. Since a large number of OTEC floaters are required, a comprehensive study must be conducted to propose the principal concept design applicable to various locations optimizing OTEC implementation, including the technical readiness of CWP [10].

An important component that needs to be developed in OTEC is the

* Corresponding author.

E-mail address: ristiyanto.adiputra@brin.go.id (R. Adiputra).

<https://doi.org/10.1016/j.rineng.2024.102863>

Received 29 June 2024; Received in revised form 7 August 2024; Accepted 5 September 2024

Available online 7 September 2024

2590-1230/© 2024 The Authors. Published by Elsevier B.V. This is an open access article under the CC BY-NC license (<http://creativecommons.org/licenses/by-nc/4.0/>).

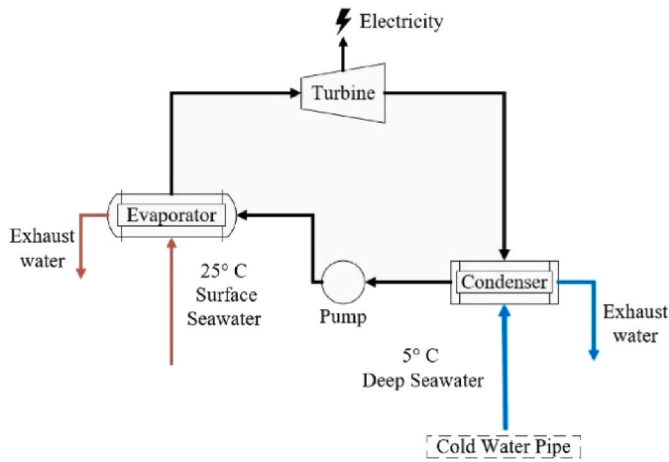


Fig. 1. The Rankine cycle in ocean thermal energy conversion (OTEC) [52].

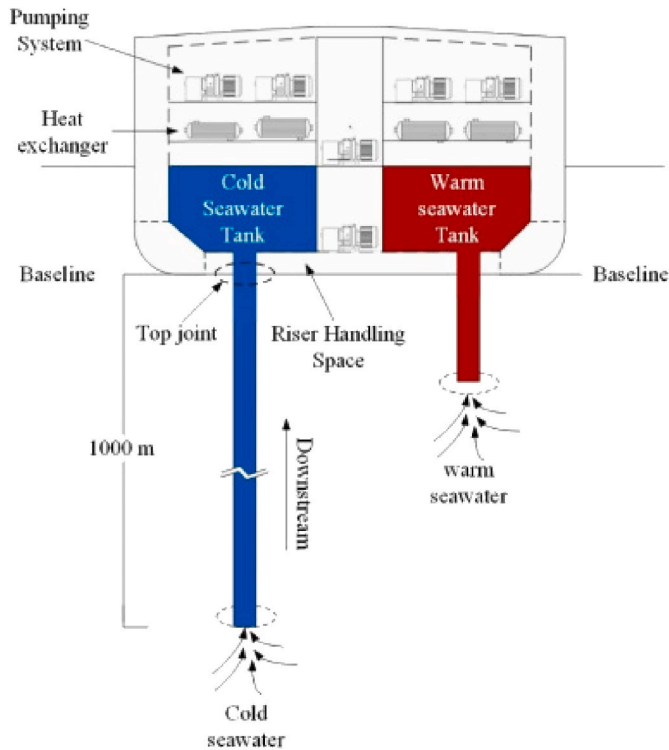


Fig. 2. The cold water and hot water input [9].

cold water pipe (CWP). This pipeline is used to transport cold water from specific ocean depths to the OTEC power generation system. The structural system used in CWP resembles the hang-off system used in offshore drilling, where both are hanging structures. Research conducted by Mao et al. states that the hang-off riser has the highest stress point when it is at the end that hits the platform and the highest deformation occurs at the free end [11]. However, the hang-off riser has a much smaller size compared to the CWP OTEC (the diameter of the hang-off riser is around 1.5 m) [12], so further study of the CWP OTEC geometry is needed to make it more similar to the actual conditions. Additionally, the addition of a ring stiffener, which may increase the durability of the pipe structure [13], should be elaborated in the CWP design.

The CWP requires special attention to the vulnerability of structural damage caused by ocean currents (C. C. K [14]). Despite its importance, literature review results in limited research have been devoted to the

structural sustainability of OTEC CWP [15]. Adiputra and Utsunomiya conducted tests involving internal fluid loads on the CWP, exploring variations in materials, geometry, top connections, and end loads [16]. In a separate study, Muhammad Iqbal et al. analyzed the impact of internal flow on the stability of CWP using developed FEM [8]. Another investigation by Prayoga Wira Adie et al. used finite element (FE) analysis to examine geometric and material variations [17].

To date, based on the authors' knowledge, no research has focused on using stiffeners to improve the durability of OTEC CWP structures. Therefore, this study aimed to explore the effect of using stiffeners on OTEC CWP subjected to bending loads. It seeks to determine the most effective stiffening regime through different geometric variations to enhance the strength of the structure [18]. A parametric configuration was also imposed in the ring stiffener design to understand how the ring stiffener's geometrical parameters influence the ultimate bending capacity.

2. Buckling phenomenon on cylindrical shell under bending load

The buckling problem of cylindrical shells has received much attention due to its important role in the design of marine structures [19]. Pipelines, during the operational phase, encounter many different loads [20]. The instability of structural members under these varying loads often leads to severe structural damage [21].

The maximum bending stress of a cylinder under the critical (buckling) moment M_{cr} can be expressed by Eq. (1) [22]:

$$\sigma_{cr} = \frac{M_{cr}}{\pi r^2 t} \quad (1)$$

where σ_{cr} is critical stress, r is the pipe radius, and t is the wall thickness. If the critical (buckling) stress of the cylinder under bending is the same as the buckling stress of the cylinder under uniform compression, the critical stress can be expressed by Eq. (2) [23]:

$$\sigma_{cr} = \frac{E}{\sqrt{3(1-\nu^2)}} \left(\frac{t}{r} \right) \quad (2)$$

where E is Young's modulus and ν is Poisson's ratio. If it is assumed that a thin-walled pipe is subjected to bending when the compressive stress reaches a value at which the stress reaches an unstable point, the critical moment can be found by combining Eq. (1) and Eq. (2) and if the material is assumed to use is steel with a Poisson's ratio of 0.3, Eq. (3) is obtained [22]:

$$M_{cr} = 0.605 \pi E r^2 t \quad (3)$$

Timoshenko and Gere [23] declared that the maximum compressive stress at the critical buckling moment is about 30 % higher than that obtained from Eq. (2):

$$M_{cr} = 0.787 \pi E r^2 t \quad (4)$$

The calculation results of Yudo and Yoshikawa [24] for a straight pipe, whose L/D varies from 5 to 20, and D/t varies from 50 to 200, showed that the critical bending moment in linear calculation is expressed by Eq. (5):

$$M_{cr} = 0.666 \pi E r^2 t \quad (5)$$

The first discovery of nonlinear structural analysis was made by Brazier. His work focuses on the problem of stability of long cylindrical shells under bending loads. When a long cylinder is bent, its cross-section tends to flatten, resulting in reduced bending stiffness. This decrease in stiffness is directly correlated with an increase in bending moment, relative to the applied curvature, reaching the maximum threshold. Brazier's analysis, although somewhat preliminary, determined the bending moment as described by Eq. (6) [22].

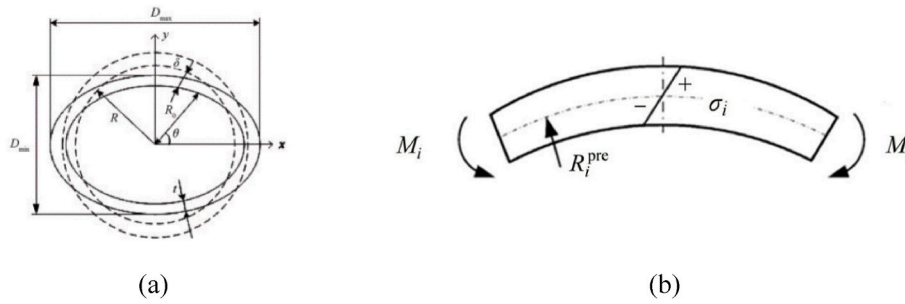


Fig. 3. Analytical concepts in this study: (a) Ovality deformation [53] dan (b) Bending curvature [31].

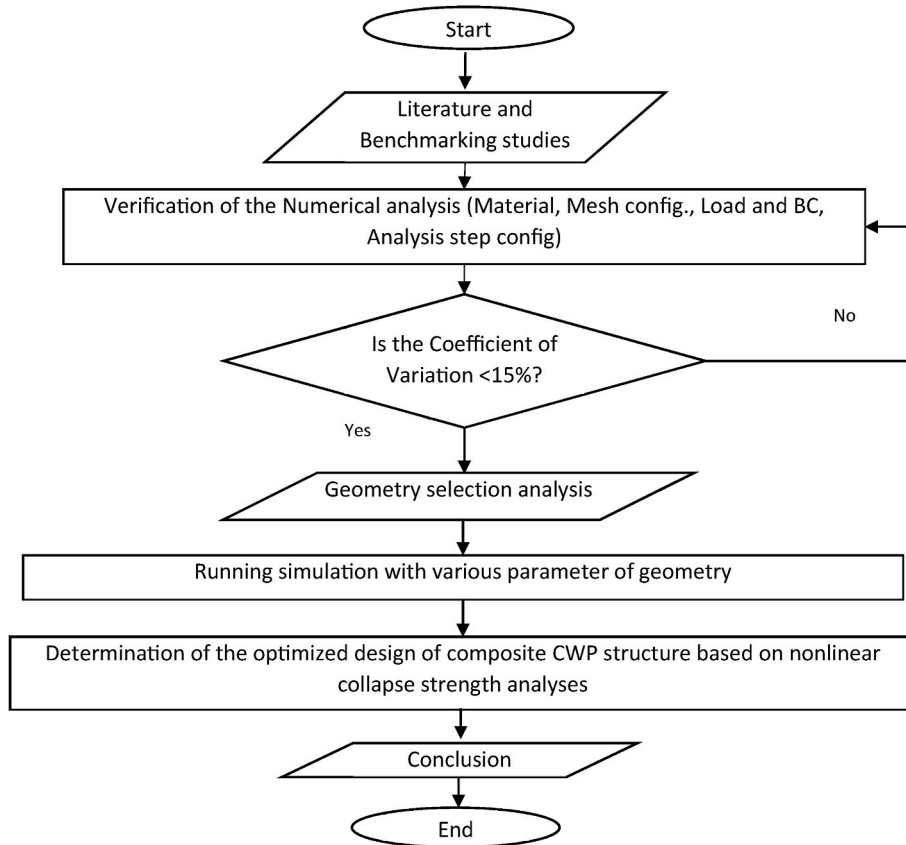


Fig. 4. Methodology of study.

$$M_{cr} = 0.329\pi E r^2 t \tag{6}$$

Despite the importance of the problem, extensive research on the buckling strength of pipes subjected to bending loads has not received much attention. This study aims to fill this gap by performing a series of calculations on the buckling and collapse resistance of straight and curved pipes during bending, using the nonlinear finite element method.

For a cylindrical shell structure attached by stiffener, the stiffener effect to the plastic bending moment is evaluated by C.A. Dimopoulos and C.J. Gantes [25]. The addition of stiffener increases the cross-sectional area of cylindrical shell. The ratio of total cross-section area of the stiffeners and the cross-section area of the cutout is considered to affect the plastic bending moment with this equation [25]:

$$M_{pl} = \frac{1}{2} \bar{A} f_y (y_t + y_b) \tag{7}$$

where \bar{A} is the area of the cross-section, f_y is the yield stress and y_t and y_b are the distances of the centres of gravity of each of the two parts of the

section above and below the plastic neutral axis. The equation of critical moment used by C.A. Dimopoulos and C.J. Gantes is (L [26]):

$$M_{cr} = \pi \left(\frac{E}{\sqrt{3(1-\nu^2)}} \left(\frac{t}{r} \right) \right) r^2 t \tag{8}$$

Another notable phenomenon observed in pipes subjected to bending loads is ovality [27], in which the initially circular plane of the pipe surface deforms into an oval shape [28]. This deformation model is shown in Fig. 3(a). Along its entire length, the pipe will have a curvature, as shown in Fig. 3(b).

3. Research milestones

Finite element method (FEM) are often preferred for assessing stress changes in structural components because they provide detailed and accurate analysis of specific areas [29]. According to Ref. [30], the finite element model effectively captured the mechanical behaviour and

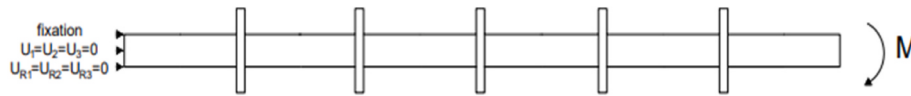


Fig. 5. The boundary conditions for the validation.

Table 1

The result of the numerical validation.

Reference	Normalized Curvature	Normalized Moment
Present Study	1.52	1.05
Yadav & Gerasimidis (2019) [41]	1.654	1.112
Difference	7.67	5.15

demonstrated a strong correlation with experimental data. The FEM is a numerical technique that models structures by dividing them into small elements, thereby forming a mesh [31]. The interactions between these elements are determined at the node level, where calculations are performed based on predefined mathematical equations [32]. FEM was used in this study due to its cost-effectiveness and flexibility to accommodate many analysis variations [33]. ABAQUS, a software specialized in FEM calculations, uses geometric and material properties to create a stiffness matrix, an important multiplier in FEM. The basic formula of the method is shown in Eq. (9) [17].

$$\{f\} = [k]\{u\} \quad (9)$$

where $\{f\}$ is the acting force, $[k]$ is matrix stiffness, and $\{u\}$ is vector nodal shape.

Several studies have been carried out on the application of reinforcement in cylindrical shell structures. Farhad and Kamal [34] analyzed the influence of ring stiffeners on the maximum buckling resistance of pipes under external load. They varied the stiffener shape into three types: R, T and L. T-shaped stiffeners have the highest strength, followed by L-shaped stiffeners and then R-shaped stiffeners. Widiyanto and colleagues [35] studied the impact of stiffness variations on the durability of offshore pipeline structures under external load. The results indicated that the incorporation of annular stiffener significantly improved the buckling resistance, while the critical buckling decreased as the diameter increased.

Ozer and Yasin [36] analyzed the effects of strengthening steel tanks using ring stiffeners under non-uniform loading. Their research found that incorporating an annular stiffener in the center significantly improved the tank's resistance to wind-induced buckling during construction. Polenta et al. [37] introduced a new type of stiffener called "clamp" to withstand bending loads, demonstrating the ability High bending load capacity. The study confirmed the significant benefits of internal pressure on buckling phenomena, this proposed structure efficiently utilized internal pressure.

Dimopoulos and Gantes [25] conducted a study comparing different types of reinforcement in wind turbine towers. They found that simpler types of reinforcement, such as two longitudinal bars with rings, were more effective than more complex types of reinforcement, such as a combination of frames, ties, and rings. Yu Hu et al. [38] used internal stiffening rings in wind turbine tower structures, by varying the dimensions of stiffener. Their results highlight that thinner wall thicknesses allow for greater strength improvements, especially at lower rates.

4. Methodology

This study uses the finite element method. The research process began with an in-depth review of the CWP OTEC literature and testing of cylindrical shell structures under bending loads, identifying the standard tests that needed to be performed. Taking advantage of the results of the literature review and benchmarking, numerical verification was

performed, referring to previous studies on cylindrical shells subjected to bending loads. Validation is performed by replicating the reference study test, ensuring that the test results agree within 15 % of the reference study results [39]. The flow of methodology of this study can be seen in Fig. 4.

4.1. Numerical validation

To confirm the validity of the current computational method and solution setup, it is necessary to demonstrate that the results are both correct and achieve the required level of accuracy within the numerical framework [40]. This validation was accomplished by replicating the study by Yadav and Gerasimidis [41] on the instability of cylindrical shell under bending load. Yadav and Gerasimidis studied a cantilever subjected to bending loads at the end of the tube, similar to the CWP OTEC scenario, where the structure represents a cantilever with a free end, resulting in similar bending loads. The study by Yadav and Gerasimidis provided comprehensive information, facilitating simple replication. They used a cylindrical hull shape with a distance between reinforcing bars of 20 m, a radius of 4 m and a thickness of 0.067 m. The material used was medium carbon steel with a yield stress (σ_y) of 355 MPa, Young's modulus (E) of 210 GPa, and Poisson's ratio of 0.3. For material input, Yadav and Gerasimidis [41] used the Ramberg–Osgood plasticity model. The Ramberg–Osgood model for carbon steel material is expressed by Eq. (10) [42].

$$\varepsilon = \frac{\sigma}{E} \left[1 + \frac{3}{7} \left(\frac{\sigma}{\sigma_y} \right)^{n-1} \right] \quad (10)$$

The boundary conditions applied is also followed Yadav and Gerasimidis [41]. Fixed ends are made on one side of the pipe, therefore $U1 = U2 = U3 = UR1 = UR2 = UR3 = 0$. On the other hand, it is a given moment load. The given moment is a rotational displacement using θ . The boundary conditions for the validation carried out can be seen in Fig. 5.

Validation was carried out using ABAQUS software using the static risk method. The result of the moment load and the curvature will be normalized. The results of the numerical validation can be seen in Table 1 and Fig. 6.

Table 1 and Fig. 6 show the difference in normalized moment and normalized curvature results between Yadav and Gerasimidis's study [41] and current research. The comparison results of curvature and bending capacity parameters fall below 8 %, indicating their similarity and that one is ready to move to the testing phase.

4.2. Mesh convergence study

Fig. 7 shows that increasing the number of elements leads to more convergent results. As the number of elements increases, the critical moments will differ from those with fewer elements. A line is added to Fig. 7 to determine the point of convergence. The graph indicates that using 12,000 elements represents the optimal mesh size. Notably, at this mesh size, the critical moment results are nearly identical to those obtained with a more significant number of elements. To improve computational efficiency, a smaller but equally efficient number of elements of 12,000 is chosen for numerical calculation (X [43]). The difference in critical moment results at different mesh sizes is due to the errors that inevitably occur when performing numerical calculations. This is because the numerical method is an approximation technique, so the different element numbers of numerical approaches performed will

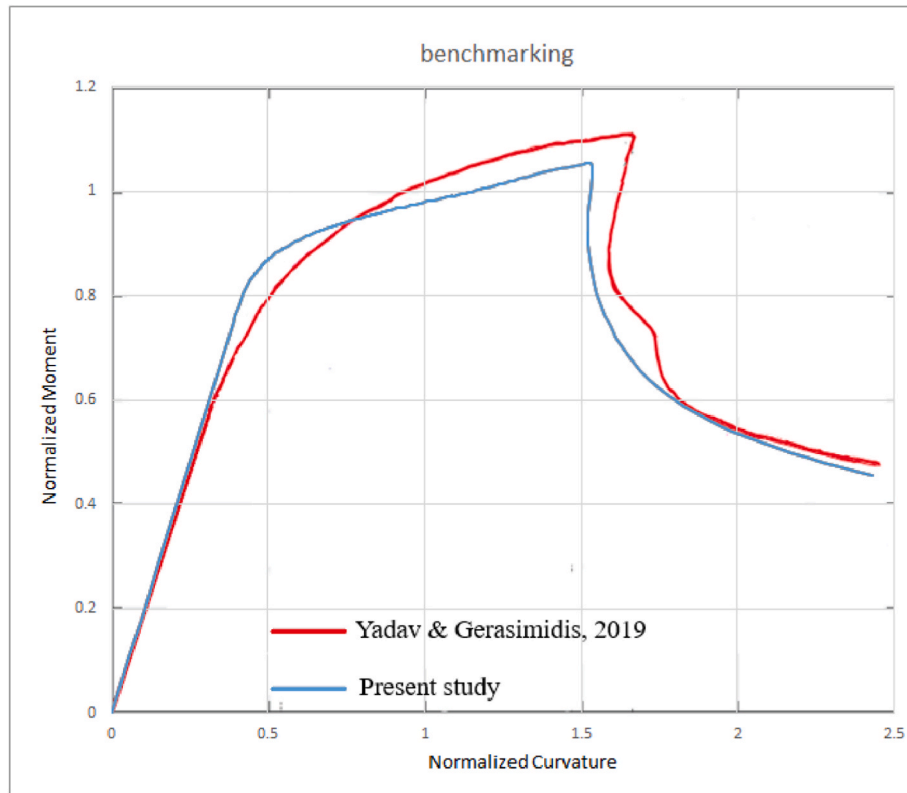


Fig. 6. Benchmarking study result.

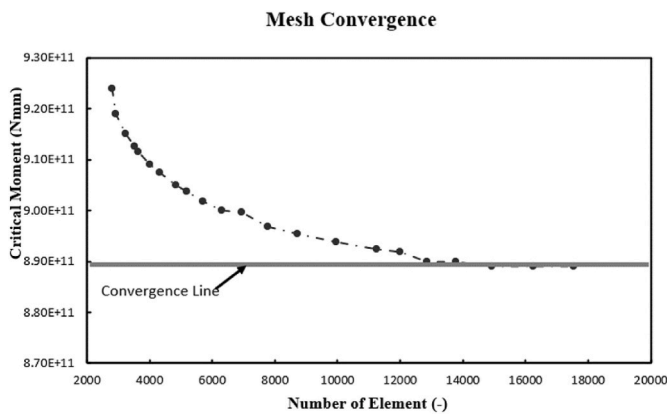


Fig. 7. The result of the mesh convergence study.

produce different results [17]. Therefore, a mesh convergence study is used so that the number of numerical runs (number of meshes) is accurate by finding the convergence point.

4.3. Numerical modeling

In this study, the numerical modeling of the CWP OTEC includes its representation as a cylindrical shell with simplified stiffeners. This approach aims to streamline numerical calculations without compromising completeness (H. T [44]). Considering the computational efficiency and the high accuracy of shell elements, the mesh modeling was done with the same SR4 meshing approach described in Section 4.1 with 120,000 elements as a reference point adopted from the results in the mesh convergence study.

The geometry used in this study is shown in Fig. 8, where the pipe diameter (D) and pipe length (L) are set to 3 m and 600 m, respectively. However, the values of stiffener thickness (t), distance between stiffeners (L0) and stiffener height vary across different iterations, according to the selected variations detailed in this section.

In ABAQUS CAE, material properties are imported related to the glass fibre reinforced polymer, including parameters such as Young's modulus, Poisson's ratio, ductility and yield strength of the material model used. These properties have a significant impact on the calculation of the ultimate moment of cylindrical shell pipes subjected to bending loads (T [45]). The plasticity of the material model in this study applies the Ramberg-Osgood model. The Ramberg-Osgood model for glass fibre reinforced polymer material is expressed by Eq. (11) [42].

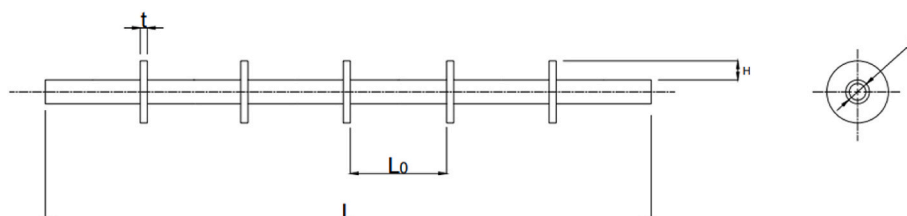


Fig. 8. Geometry used in study.

Table 2
Stiffener height variance.

Code	H/D	H (m)
A	0.1	0.3
B	0.2	0.6
C	0.3	0.9
D	0.4	1.2
E	0.5	1.5

Table 3
Stiffener thickness variance.

Code	Thickness (m)
1	0.03
2	0.02
3	0.15
4	0.12

Table 4
Stiffener spacing variance.

Code	L ₀ (m)
1	100
2	75
3	50
4	25

$$\sigma = \frac{E_0 \varepsilon}{\left(1 + \left(\frac{E_0 \varepsilon}{\sigma_0}\right)^n\right)^{1/n}} \quad (11)$$

where σ is the stress, ε is the strain, E_0 is the initial modulus of elasticity with the value of 138 GPa, σ_0 is the asymptotic stress level with the value of 100 GPa, and n is 10 [42].

The combination of ocean currents and waves causes the bending of the CWP due to the distributed loads acting on the surface of the pipe. Considering this condition, the present paper focuses on how the ring stiffener influences the bending capacity and how significantly the ring stiffener parameters contribute to increasing the ultimate capacity. Therefore, the load modeling is set as a moment load applied to the tip of the CWP, as shown in Fig. 5.

4.4. Geometry variance

There are four geometry variations used in the test. Variations in stiffener height, stiffener thickness, and stiffener spacing. Samples are coded in order of height - thickness - distance between reinforcement for each type.

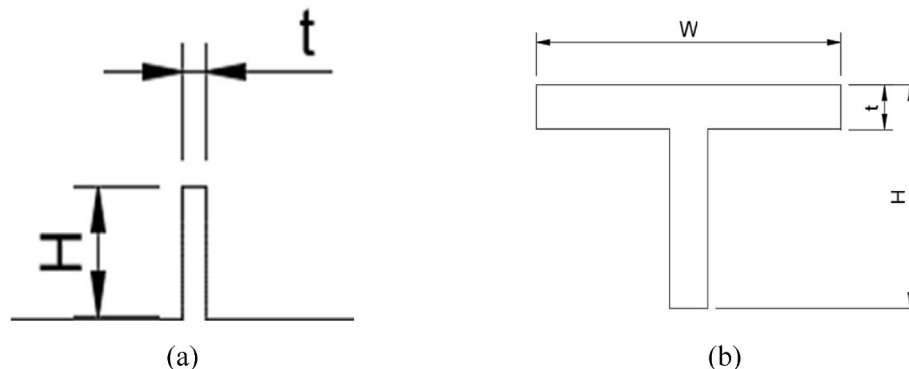


Fig. 9. Stiffener type variance: (a) Type r and (b) type T

4.4.1. Stiffener height variance

Variations in stiffener height were included in this test due to manufacturing limitations resulting from the need to produce large sizes [46]. The height of the stiffener correlates with the diameter of the CWP. The goal of this study was to reduce the height of the stiffener while maintaining optimal structural strength. The height variation used and the ratio between the height of the stiffener and the diameter of the CW are presented in Table 2.

4.4.2. Stiffener thickness variance

The variation in stiffener thickness was included in this test due to its effect on the area moment of inertia of the CWP [47]. This factor significantly affects the structural integrity and damage potential of

Table 5
Stiffener dimension for each type.

Stiffener Geometry	D (m)	H (m)	W (m)	H/D	T (m)	L1 (m)	L (m)	I (m ⁴)
R	3	1.5	-	0.5	0.03	100	1000	0.008444
T	3	0.95	1	0.5	0.03	100	1000	0.00858

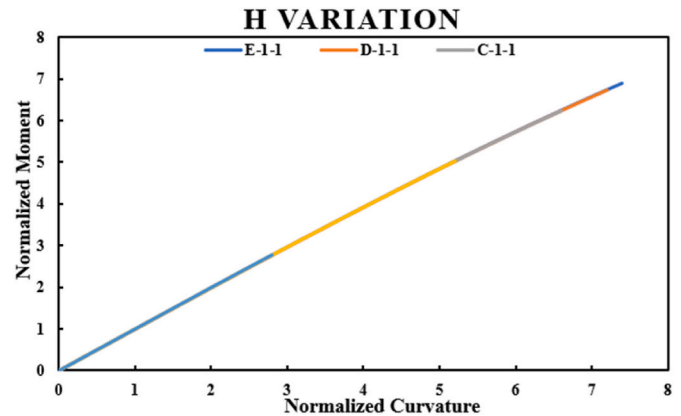


Fig. 10. Moment vs curvature for stiffener height variation.

Table 6
Critical moment for stiffener height variation.

Code	Critical Moment (Nm)
A-1-1	1.54×10^7
B-1-1	3.50×10^7
C-1-1	3.75×10^7
D-1-1	4.00×10^7
E-1-1	4.15×10^7

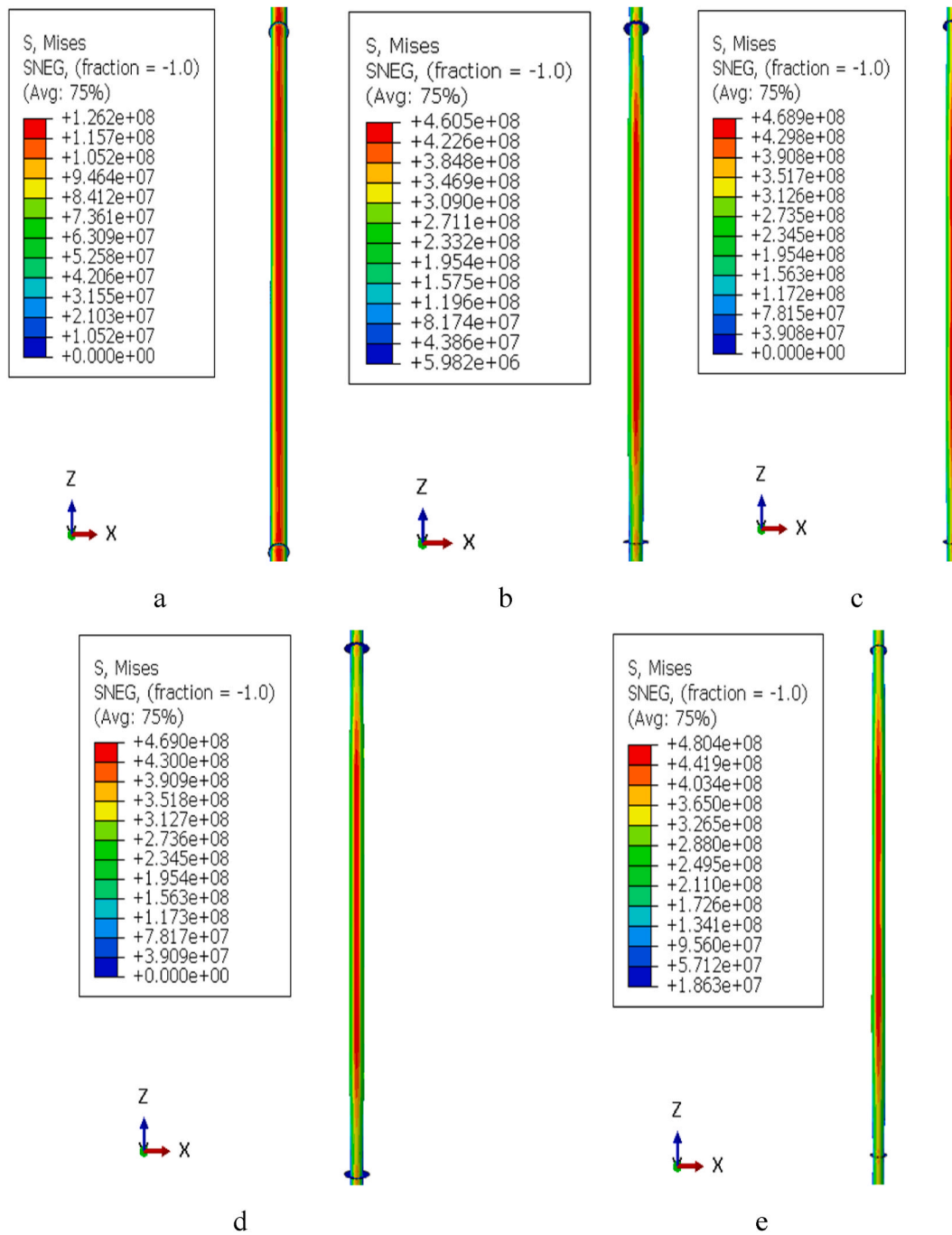


Fig. 11. Stress contours for codes: (a) A-1-1 (b) B-1-1 (c) C-1-1 (d) D-1-1 (e) E-1-1.

CWP. Details of the variation in reinforcement thickness are provided in Table 3.

4.4.3. Stiffener spacing variance

Varying the spacing between stiffeners is important in determining the number of stiffeners used [48]. The goal of this study was to determine the most effective amount of stiffener to improve structural durability. Details of the change in distance between stiffeners are given in Table 4.

4.4.4. Stiffener type variance

Variation in stiffener type is the focus of this study due to its demonstrated influence on the structural strength of cylindrical shell structures, as demonstrated by Farhad and Kamal [34]. The test

included R- and T-type stiffeners, as shown in Fig. 9. To evaluate the impact of changing splint type, dimensions were standardized for both types, as detailed in Table 5. Additionally, to determine the most optimal splint regimen, the dimensions of each splint were adjusted according to geometric variations.

5. Result and discussion

This Results and Discussion section analyses the effects of using certain variations on cylindrical casing tubes with ring reinforcement under bending loads. The observed results include the critical moment, maximum stress, and maximum displacement for each variation. Furthermore, statistical tests are performed to evaluate the influence of the variations used on the obtained results. The moment and curvature

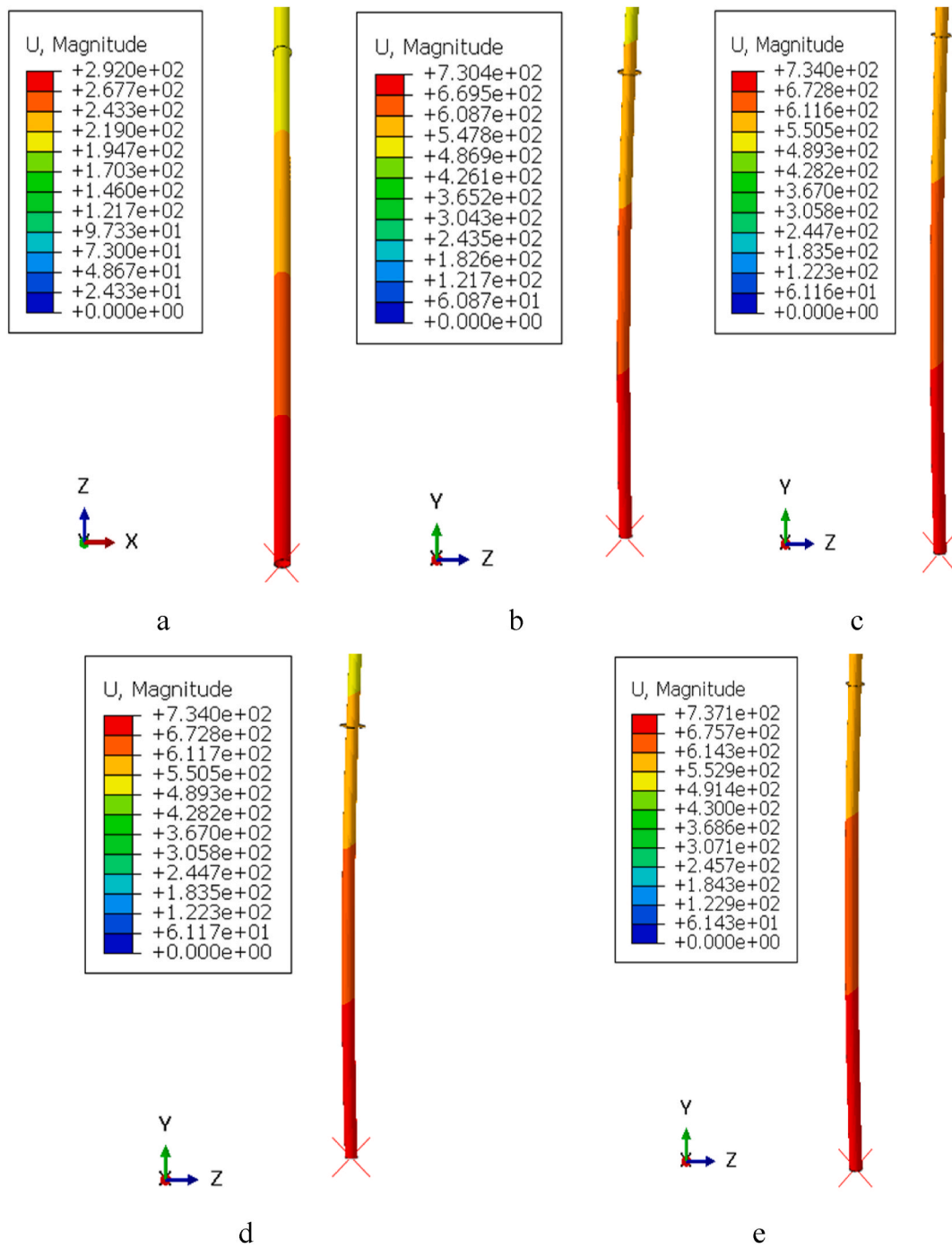


Fig. 12. Contour displacement: (a) A-1-1, (b) B-1-1, (c) C-1-1, (d) D-1-1, (e) E-1-1.

are normalized by critical moment and critical curvature for pipe without stiffener. The selection of a suitable design will be seen from the ultimate bending moment capacity, maximum stress, and displacement in the design selection. These three components are the most crucial parameters in the structural integrity of a structure to withstand the applied load in the operational state.

5.1. Stiffener height variation

The results obtained from varying the stiffener height can be seen in the moment-curvature graph shown in Fig. 10. Table 6 shows the magnitude of the critical moment for each variation.

In Fig. 10, it can be seen that the moment-curvature graph becomes

longer as the height of the ring reinforcement increases. This increases the critical moment, as shown in Table 6. The magnitude of the critical moment is affected by the moment of inertia area of the stiffener. Geometries with high stiffener heights increase the moment of inertia area of the geometry and have higher critical moments than those with lower stiffener heights. Beyond moment-curvature graphs, it is important to understand the effect of adding reinforcement on the stress and displacement contours of the structure. Figs. 11 and 12 depict the stress and displacement contours for variations in stiffener ring height.

Fig. 11 shows the stress contours at maximum stress for variations A-1-1, B-1-1, C-1-1, D-1-1, and E-1-1. The stress contours show that stiffener heights greater than 9 m have approximately the same failure contours, with failure occurring only in the middle of the pipe (indicated

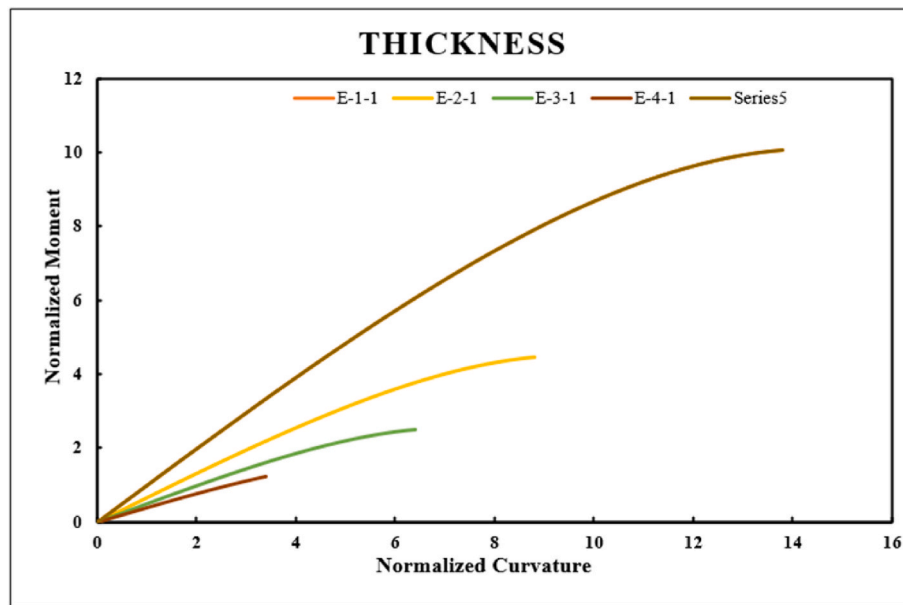


Fig. 13. Moment vs curvature thickness variation.

Table 7

Critical moment for thickness variation.

Code	Critical Moment (Nm)
E-1-1	4.15×10^7
E-2-1	2.41×10^7
E-3-1	1.66×10^7
E-4-1	7.38×10^6

by the red contour). Conversely, if the reinforcement height is 3 m, failure will occur along the length of the pipe. Additionally, the critical stress shows that the critical stress increases with higher ring reinforcement. This can be attributed to the higher critical moment of the structure, which increases the confining stress.

From the displacement contours shown in Fig. 12, using a higher ring stiffness increases the maximum displacement. This phenomenon is related to the fact that as the ring stiffness increases, the curvature increases. Curvature and maximum displacement maintain a directly proportional relationship, so an increase in curvature corresponds to an increase in maximum displacement. Looking at the moment-curvature graph, stress contours, and displacement contours, it is clear that the geometry with higher reinforcement height is more suitable for CWP OTEC reinforcement. This particular geometry was chosen because it has a high critical moment compared to other reinforcement heights, which limits the stresses and maximum displacements.

5.2. Thickness variation

The results obtained from varying the stiffener height are shown in the moment-curvature graph in Fig. 13. Table 7 shows the magnitude of the critical moment for each variation.

From the moment-curvature graph in Fig. 13, it can be seen that as the thickness increases, the moment-curvature graph becomes longer. Furthermore, by examining the critical moment quantities in Table 7, it is clear that thickness is directly proportional to the critical moment. This relationship occurs because the range of moments of inertia within the shape increases as the thickness increases. Shapes with high moment of inertia areas can withstand higher moment loads and, therefore, have higher moment resistance. The stress and displacement contours for each shape are shown in Figs. 14 and 15.

The stress contours shown in Fig. 14 indicate that using larger

thicknesses results in higher confining stresses. This is because the range of moments of inertia increases as the thickness of the geometry increases. The moment of inertia range plays an important role in absorbing moment loads, so the larger the moment of inertia range, the higher the fracture stress. Additionally, the stress contours show that defects due to thickness changes tend to occur in the center of the pipe, which is indicated by the presence of red contours.

From Fig. 15, it can be seen that the larger the thickness, the larger the maximum displacement. This is because the resulting bending length increases as the thickness increases. A direct relationship exists between curvature and displacement, so thicker geometries have higher maximum displacements.

The thickness greatly affects the overall strength of the CWP structure, which shows the same tendency with other typical applications, such as in the wind turbine tower [25] and windmill pole application [49]. In this regard, the thickness determination needs to be considered cautiously. A failure due to a lack of strength resistance can endanger not only the structure but also the operators on board [50]. Therefore, from the broader perspective, considering health and safety factors [51], it is recommended to use a large enough ring stiffener thickness so that it can withstand higher loads with the designed safety factor by preventing the occurrence of the early local buckling.

5.3. Length between stiffener variation

The results obtained from varying the stiffener height are shown in the moment-curvature graph shown in Fig. 16. Table 8 shows the magnitude of the critical moment for each variation.

In Fig. 16, it can be seen that the shorter the distance between the stiffeners, the longer the moment-curvature graph. This elongation occurs because the shorter distance between the stiffeners allows for a more uniform stress distribution [17]. The critical moment increases because the short distance between the stiffeners extends the moment-curvature relationship. The stress contours are shown in Fig. 17, and the displacement contours are shown in Fig. 18.

The stress contours shown in Fig. 17 shows that the shorter the distance between the reinforcements, the higher the upper-stress limit. This relationship is clear, as the shorter the distance between the stiffeners, the higher the critical moment. Furthermore, the stress contours show that the shorter the distance between the reinforcements, the closer the failure is to the reinforcement ring.

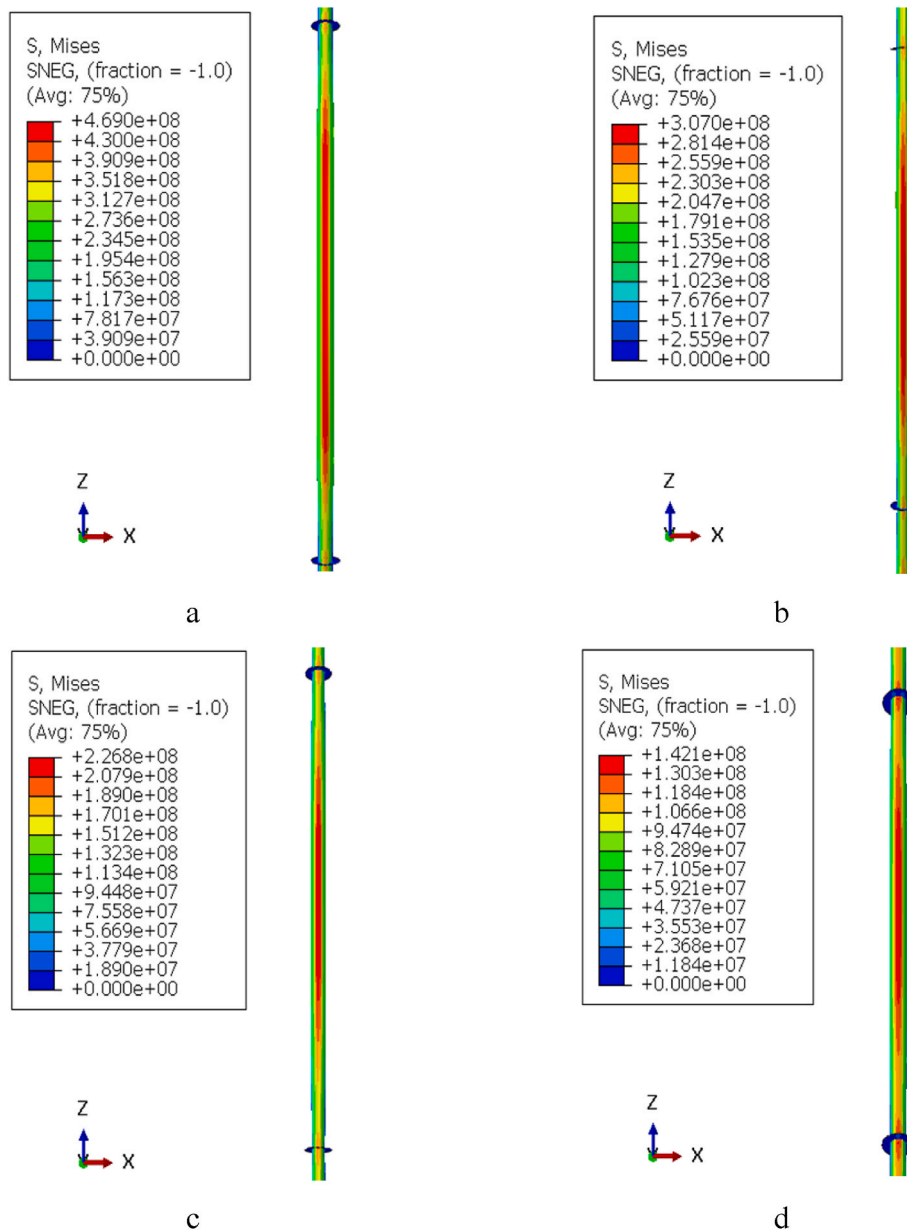


Fig. 14. Stress contours for codes: (a) E-1-1, (b) E-2-1, (c) E-3-1, (d) E-4-1.

The displacement contours show that the shorter the distance between the stiffeners in Fig. 18, the longer the maximum displacement. This relationship is evident in the moment-curvature relationship graph in Fig. 16, where the shorter the distance between the stiffeners, the greater the curvature.

Considering the moment-curvature graph, stress contours, and displacement contours together, it can be seen that the geometry with short distances between reinforcements is suitable for CWP OTEC reinforcements. This particular geometry was chosen because it has a high critical moment compared to other hardening configurations, which limits the stresses and maximum displacements.

5.4. Significant of stiffener height variation, thickness variation, and length between stiffener variation

This section examines the effects of varying the height, thickness, and spacing between stiffeners, specifically, a plot of the critical moment with respect to the change in stiffener height at different thicknesses, a plot of the critical moment with respect to the distance between the

stiffeners at different thicknesses, and the variation of the critical moment with respect to the stiffener height at the variation of stiffening system distance. Additionally, statistical analysis is performed to quantify the impact of each variation on the resulting critical moment.

Fig. 19 shows the critical moments for varying stiffener heights at different thicknesses, keeping the distance between the stiffener constant at 100 m. Consistent with the previous discussion, it is clear that a higher stiffener height corresponds to a higher critical moment. Similarly, increasing the thickness increases the critical moment. However, the effect of stiffener height decreases as thickness decreases. For example, if the thickness is 0.012 m, the difference in critical moments between reinforcement ring heights of 3 m and 1.5 m is relatively small. Furthermore, Fig. 19 shows that the effect of reinforcement thickness is greater than the height of the reinforcement on the increase in critical moment. In particular, each thickness shows clear and relatively significant differences in critical moment values compared to the change in reinforcement height.

Fig. 20 shows the critical moments at different distances between the reinforcements, considering different thicknesses and a reinforcement

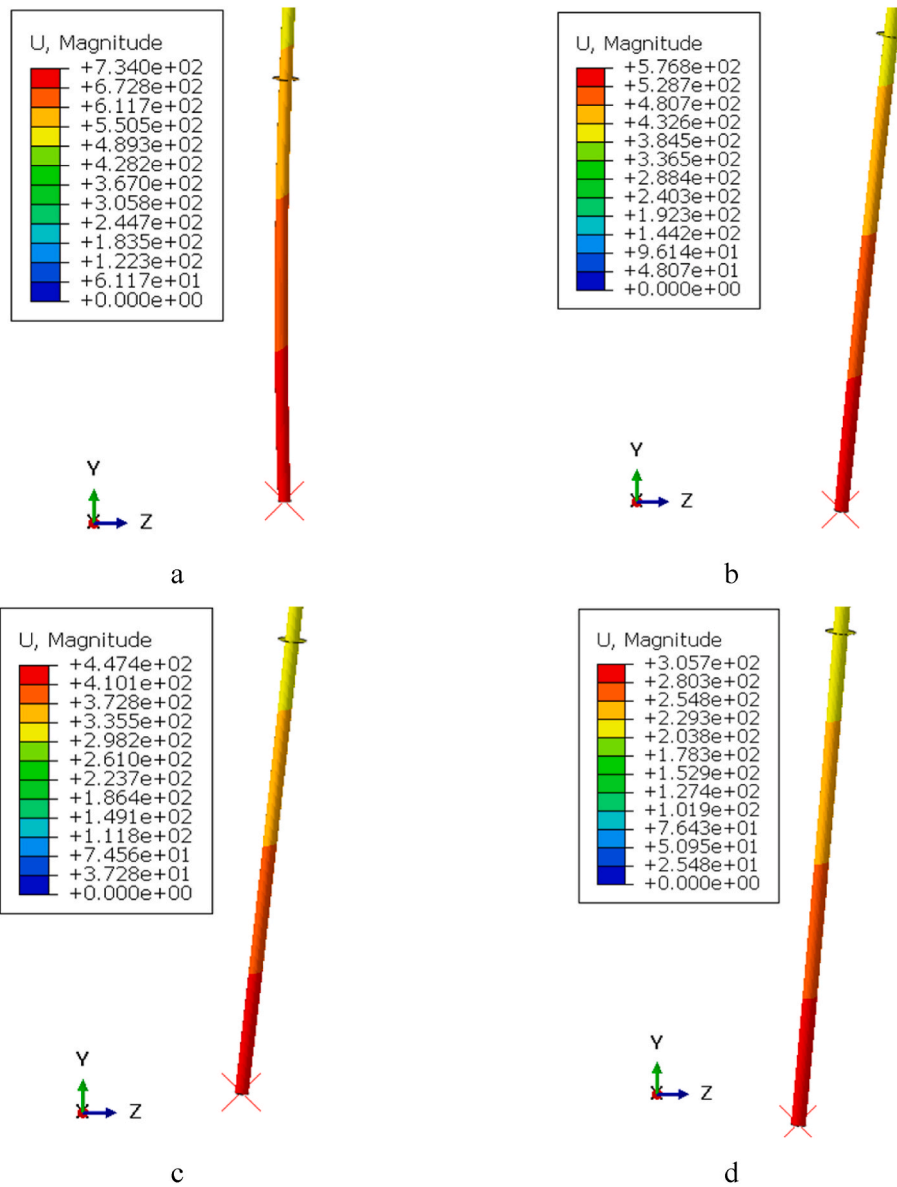


Fig. 15. Displacement contours for code: (a) E-1-1, (b) E-2-1, (c) E-3-1, (d) E-4-1.

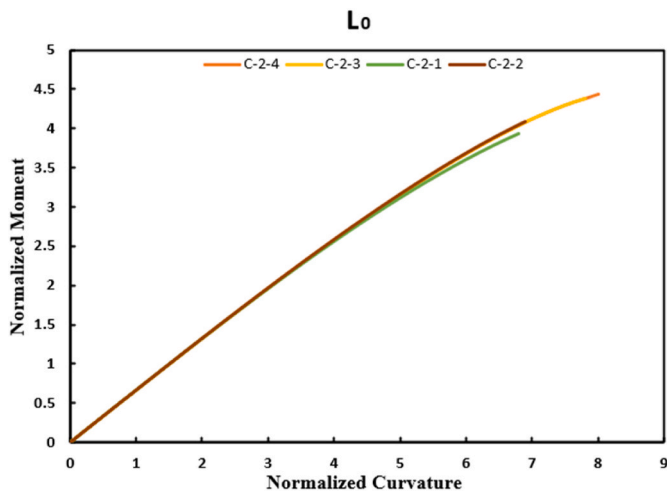


Fig. 16. Moment vs curvature graph for length between stiffener variation.

Table 8

Critical moment for length between stiffener variation.

Code	Critical Moment (Nm)
C-2-1	2.36×10^7
C-2-2	2.42×10^7
C-2-3	2.62×10^7
C-2-4	2.66×10^7

height of 0.6 m. As mentioned, the smaller the distance between the stiffeners, the higher the critical moment. The effect of thickness is consistent with the previous discussion, showing that the thicker the geometry, the higher the critical moment. Reducing the thickness, as well as varying the reinforcement height, reduces the effect of the distance between the reinforcements on the resulting critical moment. For example, at a thickness of 0.03 m, the effect of the distance between reinforcements is still clearly visible compared to a thickness of 0.12 m.

Moreover, Fig. 20 highlights that the influence of geometry thickness has a more substantial impact compared to the distance between stiffeners in generating critical moments within the geometry. The

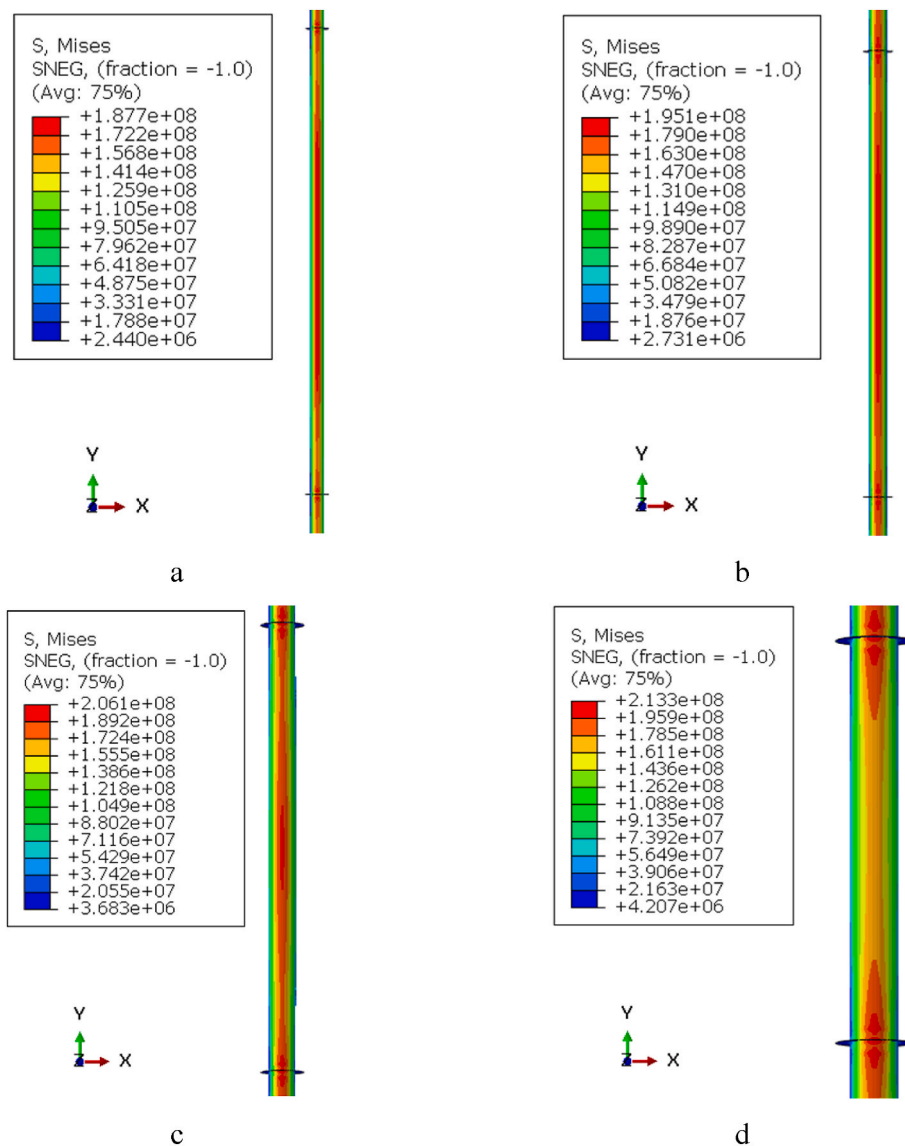


Fig. 17. Contour stress for codes: (a) C-2-1, (b) C-2-2, (c) C-2-3, (d) C-2-4.

difference in thickness produces critical moment values that significantly differ from variations in the distance between stiffeners.

Fig. 21 shows the critical moments for different reinforcement heights and distances between different reinforcements while maintaining the same thickness. As mentioned earlier, the critical moment increases as the height of the stiffeners increases, and the critical moment increases as the distance between the stiffeners decreases.

From Fig. 21, it can be seen that there is no significant difference between the effect of the height of different reinforcements and the effect of the distance between different reinforcements. This observation is supported by using different stiffener heights and no significant increase in curvature is observed. The same observation applies when using different spacing between reinforcements.

The statistical test used in this study is regression statistics, which allows us to examine the effect of each variation. Table 9 shows that among the individual variables, the thickness variable has the greatest influence, followed by the height variable, and the distance between reinforcements variable. However, when cross-joining each variable, the combination of L0 and H is the most influential variation, followed by L0 and t, and finally H and t.

Table 10 shows the correlation between the dependent and independent variables is particularly high, as indicated by the multiple R-

value of 0.975. Additionally, an R-squared value greater than 0.951 indicates that the independent variables used can effectively explain the resulting dependent variable.

5.5. Stiffener type variation

The results obtained from varying the stiffener height are shown in the moment-curvature graph shown in Fig. 22. The magnitude of the critical moment for each variation is shown in Table 11.

Table 11 shows that the critical moment values do not differ significantly for different types of reinforcement. The moment-curvature graphs in Fig. 22 also appear identical except for the critical moment points. This similarity arises because the moment of inertia areas of the two types of stiffeners are the same, as shown in Table 6. The stress contours are shown in Fig. 23 and the displacement contours are shown in Fig. 24.

As shown in Figs. 23 and 24, the displacement contours and contour tension of stiffener types show that different stiffener types do not affect the maximum displacement. Since the maximum curvatures are similar, there is no significant change either in the maximum tension or the displacement produced. However, considering the moment-curvature graph, stress contours, and displacement contours, R-type

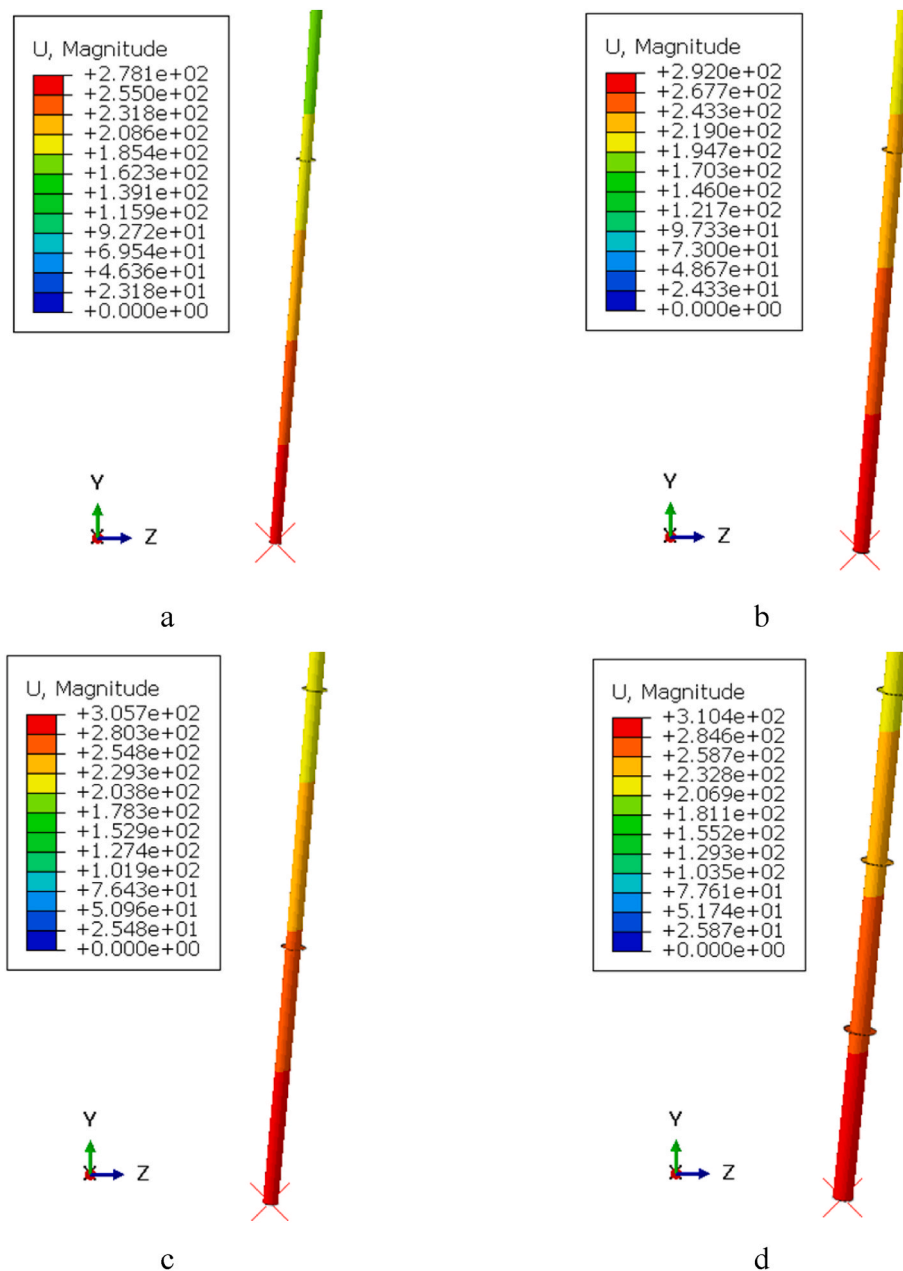


Fig. 18. Displacement contours for codes: (a) C-2-1, (b) C-2-2, (c) C-2-3, (d) C-2-4.

reinforcement is more suitable for CWP OTEC since R has comparable critical moments, stress contours, and displacement contours to Type T but with simpler manufacturing methods.

6. Conclusion

This study conducted a parametric study to determine the suitable ring reinforcement geometry for cold water pipe installation in OTEC. The finite element method was used to simulate the given geometry of the ring reinforcement. The following was observed through the simulations performed:

1. As explained in the result and discussion section, the thicker the geometry, the higher the critical moment, ultimate stress, and maximum displacement, as theoretically elaborated in section 2. An increased thickness enhances the moment of inertia area of the geometry. Hence, in CWP OTEC, a higher thickness is deemed suitable.
2. As also stated in Section 2, a cylindrical pipe will experience buckling when subjected to a bending load. The higher the height of the ring stiffener used, the higher the critical moment, ultimate stress, and maximum displacement. This is because, at larger heights, the moment of inertia area of the geometry increases. Therefore, for its use in CWP OTEC, a high stiffener ring height is recommended to withstand higher moment loads.
3. The shorter distance between stiffeners used, the greater the critical moment, ultimate stress, and maximum displacement. This is because the shorter the distance between the reinforcements, the better the load distribution within the pipe. Therefore, CWP OTEC recommends shortening the distance between reinforcements.
4. From the variations in height, thickness, and distance between reinforcements, the thickness of the ring stiffener has the most influence on the critical moment, followed by the height of the reinforcement.

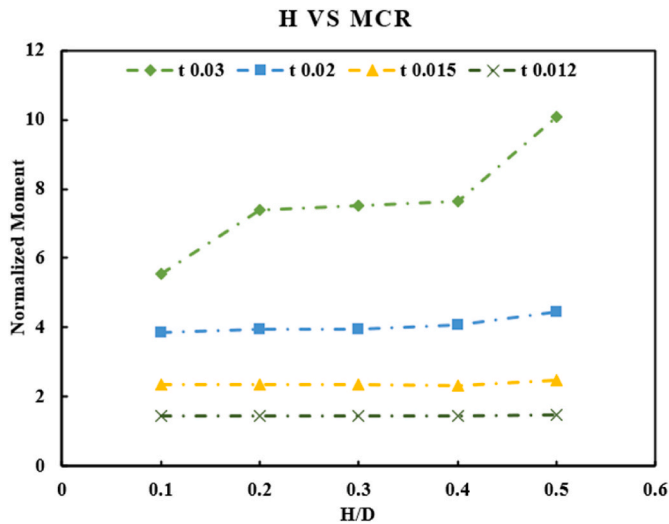


Fig. 19. Variation of stiffener height at different thicknesses.

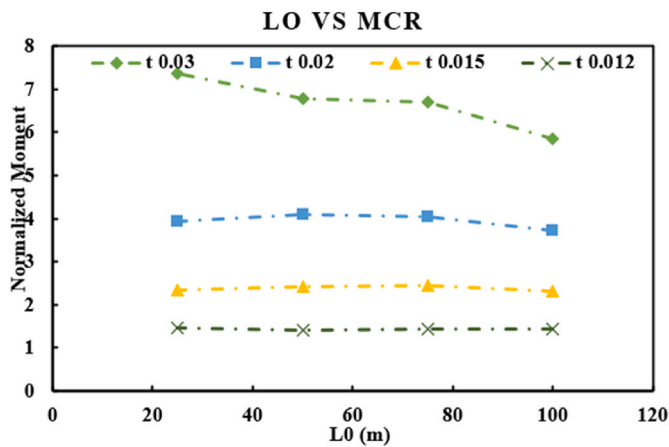


Fig. 20. Variation of spacing between stiffeners at different thicknesses.

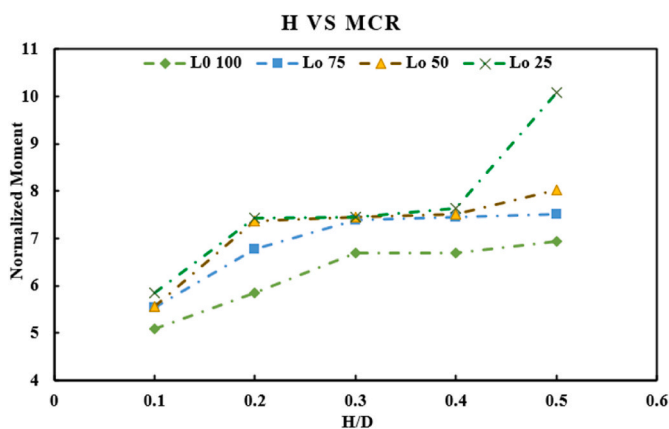


Fig. 21. Variation of stiffener height at different stiffener spacing.

5. Regarding stiffener shapes, as long as they both have the same moment of inertia area, the difference between the T-shape and the R-shape does not significantly affect the development of the critical moment that limits the critical stress and maximum displacement. Therefore, from the viewpoint of ease of manufacture, an R-type shape is preferable.

Table 9
Sensitivity of each variation.

Variation	Coefficients
L_0/L	9.56
$(L_0/L)^2$	113.96
t/D	1468.58
$(t/D)^2$	-54072.02
H/D	-10.92
$(H/D)^2$	1.97
L_0t/LD	-8564.97
$(L_0t/LD)^2$	5580411.63
L_0H/LD	-9754.57
$(L_0H/LD)^2$	-97479570.37
Ht/D^2	2586.85
$(Ht)^2/D$	-150612.67

Table 10
Regression statistic.

Regression Statistic	
Multiple R	0.975
R Square	0.951
Adjusted R Square	0.942
Standard Error	0.533

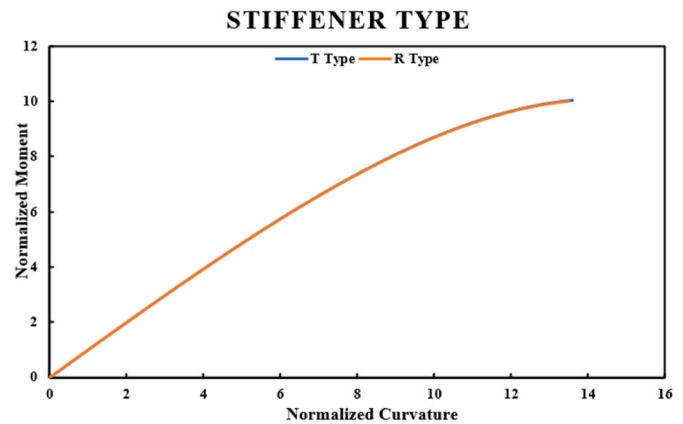


Fig. 22. Moment vs curvature stiffener type variation.

Table 11
Critical moment for stiffener type variation.

Stiffener Type	Critical Moment (Nm)
R Type	6.00×10^7
T Type	6.01×10^7

For future research, it would be beneficial to include combination loading so that the applied load is not only the bending load but also the effect of hydrostatic pressure. Dynamic loading can also be investigated to understand the fatigue behavior of the OTEC CWP structure. Additionally, in this study, the ultimate bending capacity of the pipe has been obtained through a parametric study with various geometrical configurations of the ring stiffener. The tendency of the ring stiffener parameter to influence the ultimate bending capacity has also been obtained. To select the CWP configuration, the analysis-based operational state should be conducted for site-specific cases and compared with the ultimate bending capacity, resulting in this study with a determined safety factor.

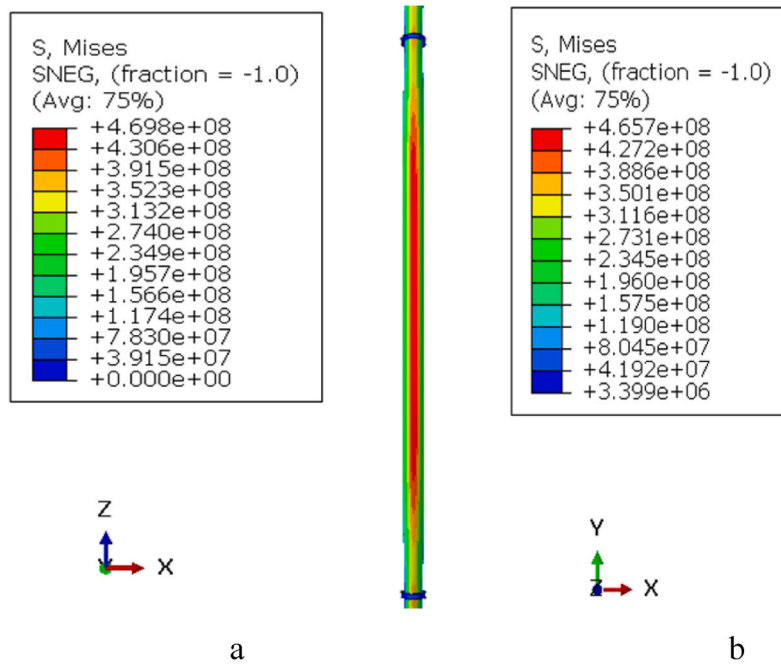


Fig. 23. Contour tension type stiffeners: (a) T-type, (b) R-type.

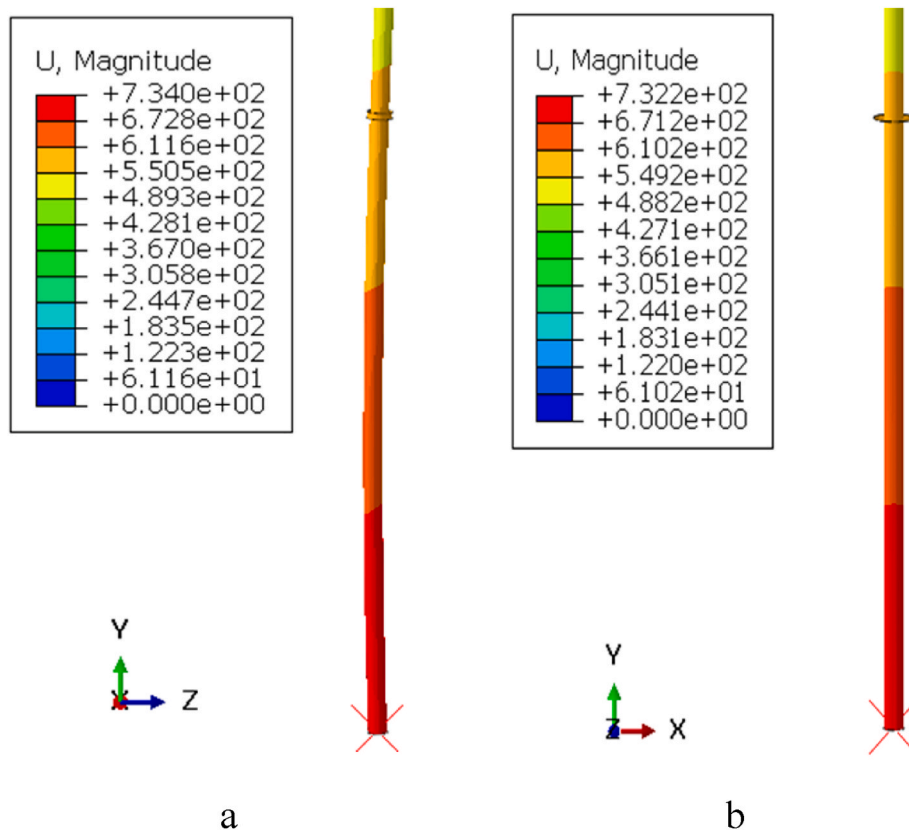


Fig. 24. Displacement contour of stiffener type: (a) T-type, (b) R-type.

CRedit authorship contribution statement

Rasgianti: Writing – review & editing, Writing – original draft, Visualization, Project administration, Investigation, Formal analysis, Writing – review & editing, Writing – original draft, Visualization, Project administration, Investigation, Formal analysis. **Ristiyanto**

Adiputra: Writing – review & editing, Writing – original draft, Validation, Methodology, Investigation, Formal analysis, Conceptualization. **Ariyana Dwiputra Nugraha:** Validation, Supervision, Project administration, Funding acquisition, Formal analysis. **Nurman Firdaus:** Software, Methodology, Investigation, Conceptualization. **Rully Bayu Sitanggang:** Writing – review & editing, Supervision, Resources, Project

administration. **Navik Puryantini**: Software, Project administration, Methodology, Funding acquisition, Formal analysis. **Takeshi Yasunaga**: Supervision, Methodology, Conceptualization.

Declaration of competing interest

The authors declare that they have no known competing financial interests or personal relationships that could have appeared to influence the work reported in this paper.

Data availability

Data will be made available on request.

Acknowledgments

This work is part of the OTEC research activity “Cold Water Pipe (CWP) Design for 5 MW OTEC Plant: Study Case of North Bali” Research Grand DIPA No. DIPA-124.01.1.690505/2024 conducted by the Marine Renewable Energy research group, Research Center for Hydrodynamics Technology, National Research and Innovation Agency (BRIN). Collaboration with PT. PLN Research Institute is highly acknowledged

References

- [1] E. Bushra, K. Zeb, I. Ahmad, M. Khalid, A comprehensive review on recent trends and future prospects of PWM techniques for harmonic suppression in renewable energies based power converters, *Results in Engineering* 22 (April) (2024) 102213, <https://doi.org/10.1016/j.rineng.2024.102213>.
- [2] H. Queiroz, R.A. Lopes, J. Martins, F.N. Silva, L. Fialho, N. Bilo, Assessment of energy sharing coefficients under the new Portuguese renewable energy communities regulation, *Heliyon* 9 (10) (2023) e20599, <https://doi.org/10.1016/j.heliyon.2023.e20599>.
- [3] Rasgianti, R. Adiputra, A.D. Nugraha, R.B. Sitanggang, W.W. Pandoe, Aprjanto, T. Yasunaga, M.A. Santosa, System parameters sensitivity analysis of Ocean Thermal energy conversion, *Emerging Science Journal* 8 (2) (2024), <https://doi.org/10.28991/ESJ-2024-08-02-04>.
- [4] J. Langer, J. Quist, K. Blok, Upscaling scenarios for ocean thermal energy conversion with technological learning in Indonesia and their global relevance, *Renew. Sustain. Energy Rev.* 158 (2022) 112086, <https://doi.org/10.1016/j.rser.2022.112086>.
- [5] Q. Ma, Z. Gao, J. Huang, O. Mahian, X. Feng, H. Lu, S. Wang, C. Wang, R. Tang, J. Li, Thermodynamic analysis and turbine design of a 100 kW OTEC-ORC with binary non-azeotropic working fluid, *Energy* 263 (2023) 126097, <https://doi.org/10.1016/j.energy.2022.126097>.
- [6] Y.M. Lutfi, R. Adiputra, A.R. Prabowo, T. Utsunomiya, E. Erwandi, N. Muhayat, Assessment of the stiffened panel performance in the OTEC seawater tank design: parametric study and sensitivity analysis, *Theoretical and Applied Mechanics Letters* 13 (4) (2023) 100452, <https://doi.org/10.1016/j.taml.2023.100452>.
- [7] Z. Wu, H. Feng, L. Chen, Z. Xie, C. Cai, S. Xia, Optimal design of dual-pressure turbine in OTEC system based on structural theory, *Energy Convers. Manag.* 201 (2019) 112179, <https://doi.org/10.1016/j.enconman.2019.112179>.
- [8] M.I. Habib, R. Adiputra, A.R. Prabowo, E. Erwandi, N. Muhayat, T. Yasunaga, S. Ehlers, M. Braun, Internal flow effects in OTEC cold water pipe: finite element modelling in frequency and time domain approaches, *Ocean Eng.* 288 (2023) 116056, <https://doi.org/10.1016/j.oceaneng.2023.116056>.
- [9] R. Adiputra, T. Utsunomiya, J. Koto, T. Yasunaga, Y. Ikegami, Preliminary design of a 100 MW-net ocean thermal energy conversion (OTEC) power plant study case: Mentawai island, Indonesia, *J. Mar. Sci. Technol.* 25 (1) (2020) 48–68, <https://doi.org/10.1007/s00773-019-00630-7>.
- [10] A. Giostri, A. Romei, M. Binotti, Off-design performance of closed OTEC cycles for power generation, *Renew. Energy* 170 (2021) 1353–1366, <https://doi.org/10.1016/j.renene.2021.02.047>.
- [11] L. Mao, S. Zeng, Q. Liu, G. Wang, Y. He, Dynamical mechanics behavior and safety analysis of deep water riser considering the normal drilling condition and hang-off condition, *Ocean Eng.* 199 (2020) 106996, <https://doi.org/10.1016/j.oceaneng.2020.106996>.
- [12] L. Xu, J. Wang, Y. Li, L. Sheng, C. Li, J. Liu, M. Li, X. Liu, Development and sea trial investigation for deepwater drilling riser specialized soft hang-off system during transit, *Ocean Eng.* 243 (2022) 110310, <https://doi.org/10.1016/j.oceaneng.2021.110310>.
- [13] N. Rathinam, B. Prabu, N. Anbazhagan, Buckling analysis of ring stiffened thin cylindrical shell under external pressure, *J. Ocean Eng. Sci.* 6 (4) (2021) 360–366, <https://doi.org/10.1016/j.joes.2021.03.002>.
- [14] C.C.K. Liu, Ocean thermal energy conversion and open ocean mariculture: the prospect of Mainland-Taiwan collaborative research and development, *Sustainable Environment Research* 28 (6) (2018) 267–273, <https://doi.org/10.1016/j.serj.2018.06.002>.
- [15] Y. Matsuda, D. Suyama, T. Sugi, S. Goto, T. Yasunaga, Y. Ikegami, Construction of a state space model for an OTEC plant using Rankine cycle with heat flow rate dynamics, *IFAC-PapersOnLine* 53 (2) (2020) 13042–13047, <https://doi.org/10.1016/j.ifacol.2020.12.2174>.
- [16] R. Adiputra, T. Utsunomiya, Finite element modelling of ocean thermal energy conversion (OTEC) cold water pipe (CWP), *Int. Conf. Offshore Mech. Arctic Eng.* 85888 (2022) V004T05A012.
- [17] P.W. Adie, A.R. Prabowo, T. Muttaqie, R. Adiputra, N. Muhayat, H. Carvalho, N. Huda, Non-linear assessment of cold water pipe (CWP) on the ocean thermal energy conversion (OTEC) installation under bending load, *Procedia Struct. Integr.* 47 (2023) 142–149, <https://doi.org/10.1016/j.prostr.2023.07.005>.
- [18] M.I. Maulana, A.R. Prabowo, T. Muttaqie, N. Muhayat, D.D.D.P. Tjahjana, Q.T. Do, J.M. Sohn, H. Nubli, Analysis of the idealized steel pipe under internal explosive loading: comparison between FE approach and laboratory experiment, *Procedia Struct. Integr.* 47 (2023) 150–158, <https://doi.org/10.1016/j.prostr.2023.07.006>.
- [19] V. Ravulapalli, G. Raju, V. Narayanamurthy, Experimental and numerical studies on the elasto-plastic buckling response of cylindrical shells with spigot support under axial compression, *Thin-Walled Struct.* 191 (2023) 111095, <https://doi.org/10.1016/j.tws.2023.111095>.
- [20] R. Naseri Ghalghachi, H. Showkati, S. Eyyavazinejad Firouzsalari, Experimental, numerical and analytical study on axial compression buckling of chopped glass fibre-reinforced polymer cylindrical shells, *Structures* 58 (2023) 105368, <https://doi.org/10.1016/j.istruc.2023.105368>.
- [21] Y. Zhu, W. Guan, W. Wang, C. Dong, J. Zhang, Buckling performance of stiffened polymer composite cylindrical shell, *Eng. Struct.* 295 (2023) 116848, <https://doi.org/10.1016/j.engstruct.2023.116848>.
- [22] V. Polenta, S.D. Garvey, D. Chronopoulos, A.C. Long, H.P. Morvan, Optimal internal pressurisation of cylindrical shells for maximising their critical bending load, *Thin-Walled Struct.* 87 (2015) 133–138, <https://doi.org/10.1016/j.tws.2014.11.012>.
- [23] S.P. Timoshenko, J.M. Gere. *Theory of elastic stability*, 2nd ed., Courier Corporation, 2009, pp. 440–453.
- [24] H. Yudo, T. Yoshikawa, Buckling phenomenon for straight and curved pipe under pure bending, *J. Mar. Sci. Technol.* 20 (1) (2015) 94–103, <https://doi.org/10.1007/s00773-014-0254-5>.
- [25] C.A. Dimopoulos, C.J. Gantes, Comparison of stiffening types of the cutout in tubular wind turbine towers, *J. Constr. Steel Res.* 83 (2013) 62–74, <https://doi.org/10.1016/j.jcsr.2012.12.016>.
- [26] L. Chen, C. Doerich, J.M. Rotter, A study of cylindrical shells under global bending in the elastic-plastic range, *Steel Construction* 1 (1) (2008) 59–65, <https://doi.org/10.1002/stco.200890008>.
- [27] A.M. Naufal, A.R. Prabowo, T. Muttaqie, A. Hidayat, R. Adiputra, N. Muhayat, S. Hadi, I. Yaningsih, Three-point bending assessment of cold water pipe (CWP) sandwich material for ocean thermal energy conversion (OTEC), *Procedia Struct. Integr.* 47 (2023) 133–141, <https://doi.org/10.1016/j.prostr.2023.07.004>.
- [28] Y. Zhao, P. Ma, Y. Chen, K. Liu, X. Yan, B. Ma, F. Wang, Stability assessment of CIPP liner under varied boundary conditions: a theoretical and simulation study, *Results in Engineering* 22 (April) (2024) 102187, <https://doi.org/10.1016/j.rineng.2024.102187>.
- [29] S. Hussain, P.S. Chen, D. Hassanlou, M. Bolhassani, C. Bedon, Bending and lateral-torsional buckling investigation on glass beams for frameless domes, *Results in Engineering* 21 (February) (2024) 101962, <https://doi.org/10.1016/j.rineng.2024.101962>.
- [30] D.A. Varma, L. Joseph, M.K. Madhavan, K. Jayanarayanan, A. Pegoretti, Strength, durability and finite element analysis of hybrid jute/basalt fiber reinforced polymer confined concrete column under axial compression, *Results in Engineering* 22 (April) (2024), <https://doi.org/10.1016/j.rineng.2024.102281>.
- [31] T. Zhang, L. Li, S. hong Lu, J. bin Zhang, Z. Zhou, H. Gong, Effect of prestressed ultrasonic peen forming parameters on bending curvature and spherical deformation of plate, *Trans. Nonferrous Metals Soc. China* 29 (2) (2019) 270–278, [https://doi.org/10.1016/S1003-6326\(19\)64936-8](https://doi.org/10.1016/S1003-6326(19)64936-8).
- [32] K. Sakkampang, C. Sakkampang, D. Sakkampang, An experimental study and finite element analysis of the parametric of circular honeycomb core, *J. Mech. Behav. Mater.* 31 (1) (2022) 98–111, <https://doi.org/10.1515/jmbm-2022-0011>.
- [33] R. Ridwan, W. Nuriana, A.R. Prabowo, Energy absorption behaviors of designed metallic square tubes under axial loading: experiment-based benchmarking and finite element calculation, *J. Mech. Behav. Mater.* 31 (1) (2022) 443–461, <https://doi.org/10.1515/jmbm-2022-0052>.
- [34] S. Peroti, F. Riahi, M. Ghaemian, K. Rahmani, N.H. Fatemi, Numerical analysis of ring-stiffener effect on ultimate buckling strength of pipeline, *Middle East J. Sci. Res.* 13 (5) (2013) 579–584, <https://doi.org/10.5829/idosi.mejsr.2013.13.5.3339>.
- [35] I. Widiyanto, A.R. Prabowo, T. Muttaqie, N. Muhayat, I. Yaningsih, D.D.D. P. Tjahjana, W.E. Juwana, T. Miyazaki, Effects of geometry and material factors on the behavior of stiffened offshore pipe structures under hydrostatic pressure, *Journal of Applied Engineering Science* 20 (4) (2022) 1103–1121, <https://doi.org/10.5937/jaes0-38728>.
- [36] Ö. Zeybek, Y.O. Özkılıç, Effects of reinforcing steel tanks with intermediate ring stiffeners on wind buckling during construction, *J. Constr. Steel Res.* 203 (2023) 107832, <https://doi.org/10.1016/j.jcsr.2023.107832>.
- [37] V. Polenta, S.D. Garvey, D. Chronopoulos, A.C. Long, H.P. Morvan, Novel stiffeners exploiting internal pressurisation to enhance buckling behaviour under bending loads, *Thin-Walled Struct.* 105 (2016) 81–89, <https://doi.org/10.1016/j.tws.2016.04.002>.

- [38] Y. Hu, J. Yang, C. Baniotopoulos, Repowering steel tubular wind turbine towers enhancing them by internal stiffening rings, *Energies* 13 (7) (2020), <https://doi.org/10.3390/en13071538>.
- [39] S. Iqbal, T. Jamil, S. Murtuza Mehdi, Numerical simulation and validation of MWCNT-CFRP hybrid composite structure in lightweight satellite design, *Compos. Struct.* 303 (2023) 116323, <https://doi.org/10.1016/J.COMPSTRUCT.2022.116323>.
- [40] M. Tauviqirrahman, M. Muchammad, T. Setiazi, B. Setiyana, J. Jamari, Analysis of the effect of ventilation hole angle and material variation on thermal behavior for car disc brakes using the finite element method, *Results in Engineering* 17 (2023), <https://doi.org/10.1016/j.rineng.2022.100844> (October 2022).
- [41] K. Kumar Yadav, S. Gerasimidis, Instability of thin steel cylindrical shells under bending, *Thin-Walled Struct.* 137 (2019) 151–166, <https://doi.org/10.1016/J.TWS.2018.12.043>.
- [42] S. Kyriakides, A. Ok, E. Corona, Localization and propagation of curvature under pure bending in steel tubes with Lüders bands, *Int. J. Solid Struct.* 45 (10) (2008) 3074–3087, <https://doi.org/10.1016/J.IJSOLSTR.2008.01.013>.
- [43] X. Wang, W. Ma, Rational reparameterization of unstructured quadrilateral meshes for isogeometric analysis with optimal convergence, *Comput. Math. Appl.* 151 (2023) 304–325, <https://doi.org/10.1016/J.CAMWA.2023.09.050>.
- [44] H.T. Chen, S.C. Chang, M.H. Hsu, C.H. You, Experimental and numerical study of innovative plate heat exchanger design in simplified hot box of SOFC, *Int. J. Heat Mass Tran.* 181 (2021) 121880, <https://doi.org/10.1016/J.IJHEATMASSTRANSFER.2021.121880>.
- [45] T. Wang, J. Ye, Numerical analysis of bending property of bi-modulus materials and a new method for measurement of tensile elastic modulus, *J. Rock Mech. Geotech. Eng.* 15 (10) (2023) 2539–2555, <https://doi.org/10.1016/J.JRMGE.2023.03.003>.
- [46] B. Kövesdi, L. Dunai, H. Pasternak, Z. Li, R. Oly, P. Márái, Design of partial height web stiffeners in beam-to-column joints and influence of residual stresses induced by welding, *Results in Engineering* 18 (2023) 101042, <https://doi.org/10.1016/J.RINENG.2023.101042>.
- [47] M. Kılıç, M. Sagioglu Maali, M. Maali, A. Cüneyt Aydın, Experimental and numerical investigation of semi-rigid behavior top and seat T-Section connections with different triangular designed stiffener thicknesses, *Eng. Struct.* 289 (2023) 116216, <https://doi.org/10.1016/J.ENGSTRUCT.2023.116216>.
- [48] S. Ebrahimi, H. Shakib, M. Soltani, S.M. Zahrai, Hysteretic behavior of link beams with different cross-sections and stiffener arrangements, *J. Constr. Steel Res.* 170 (2020) 106084, <https://doi.org/10.1016/J.JCSR.2020.106084>.
- [49] Y. Hu, C. Baniotopoulos, J. Yang, Effect of internal stiffening rings and wall thickness on the structural response of steel wind turbine towers, *Eng. Struct.* 81 (2014) 148–161, <https://doi.org/10.1016/J.ENGSTRUCT.2014.09.015>.
- [50] F. Homaei, M. Najafzadeh, A reliability-based probabilistic evaluation of the wave-induced scour depth around marine structure piles, *Ocean Eng.* 196 (2020) 106818, <https://doi.org/10.1016/J.OCEANENG.2019.106818>.
- [51] S. Koley, Role of fluid dynamics in infectious disease transmission: insights from COVID-19 and other pathogens, *Trends in Sciences* 21 (8) (2024) 8287, <https://doi.org/10.48048/tis.2024.8287>.
- [52] W. Liu, X. Xu, F. Chen, Y. Liu, S. Li, L. Liu, Y. Chen, A review of research on the closed thermodynamic cycles of ocean thermal energy conversion, *Renew. Sustain. Energy Rev.* 119 (2020) 109581, <https://doi.org/10.1016/J.RSER.2019.109581>.
- [53] Z. Li, K. chun Shen, X. hu Zhang, G. Pan, Buckling of composite cylindrical shells with ovality and thickness variation subjected to hydrostatic pressure, *Defence Technology* 18 (5) (2022) 862–875, <https://doi.org/10.1016/J.DT.2021.06.011>.